Molecular-Resolution Imaging of Interfacial Solvation of Electrolytes for Lithium-Ion Batteries by Frequency Modulation Atomic Force Microscopy

Yuji Yamagishi[1], Hiroaki Kominami[2], Kei Kobayashi[2], Yuki Nomura[1], Emiko Igaki[1], Hirofumi Yamada[2]*

[1] Applied Materials Technology Center, Panasonic Holdings Corporation, 3-1-1 Yagumo-nakamachi, Moriguchi, Osaka 570-8501, Japan

[2] Department of Electronic Science and Engineering, Kyoto University, Katsura, Nishikyo, Kyoto 615-8510, Japan

*E-mail: yamagishi.yuji001@jp.panasonic.com

KEYWORDS: solid/liquid interface, atomic force microscopy, lithium-ion battery, solvation

ABSTRACT: Solvation structures formed by ions and solvent molecules at solid/electrolyte interfaces affects the energy storage performance of electrochemical devices, such as lithium-ion batteries. In this study, the molecular-scale solvation structures of an electrolyte, a solution of lithium bis(trifluoromethanesulfonyl)imide in propylene carbonate at the electrolyte-mica interface, were measured using frequency-modulation atomic force microscopy (FM-AFM). The spacing of the characteristic force oscillation in the force versus distance curves increased with increasing ion concentration, suggesting an increase in the effective size of molecules at the interface. Molecular dynamics simulations showed that the effective size of molecular assemblies, namely solvated ions formed at the interface, increased with increasing ion concentrations, which was consistent with the experimental results. Knowledge of molecular-scale structures of solid/electrolyte interfaces obtained by a combination of FM-AFM and molecular dynamics simulations is important in the design of electrolytes for future energy devices and in improving their properties.

TOC GRAPHICS

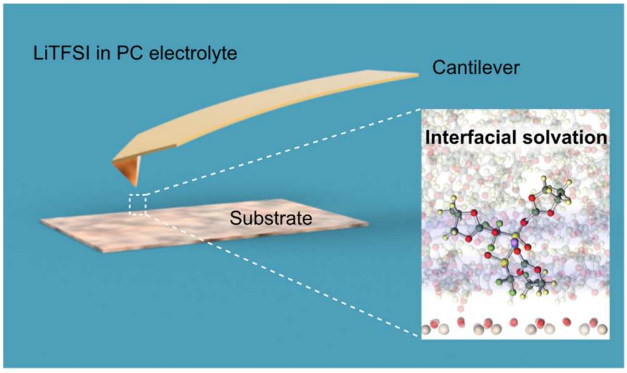

The solid/liquid interface plays an important role as a site for various chemical and biochemical reactions, such as crystal growth and catalytic reactions. In the field of electrochemistry, the solvation structure or electric double layer formed by ions and solvent molecules at the solid/liquid interface is intrinsically important because it is directly related to the performance of energy-storage devices, such as secondary batteries and catalysts. In lithium-ion batteries (LIBs), which have attracted much attention in recent years as power sources for electric vehicles and portable electronic devices, the charge transport process at the electrode/electrolyte interface is one of the factors that determines the input/output characteristics of the battery during high-speed charging and discharging, together with the transport process of Li ions in the electrolyte and the ion diffusion process in the active material particles.[1–3] In the electrolyte of LIBs, Li ions are solvated by solvent molecules and transported in the electrolyte during charging and discharging of the battery. When the solvated Li ions reach the electrode surface, they are desolvated near the surface, and Li ions are inserted into the electrode. It has been shown that the activation energy of the charge transfer reaction at the interface agrees well with the desolvation energy of Li ions calculated by density functional theory (DFT).[4–6] Therefore, the desolvation process at the interface is considered the rate-limiting process of charge transport at the electrode/electrolyte interface; hence, clarification of the molecular-scale solvation structure of the electrolyte near the solid surface is important for improving the performance of LIBs.

In recent years, the solvation structure at the solid-liquid interface has been investigated by X-ray reflectometry[7–9] and sum frequency generation.[10–12] For example, X-ray reflectometry can precisely measure the one-dimensional structure of solvation shells in the direction perpendicular to the interface, but it cannot provide information in the plane parallel to the interface; thus, it is difficult to evaluate the solvation structure in a specific area of concern. There is also a growing interest in the evaluation of high-resolution solid-liquid interfaces using atomic force microscopy.[13] Especially, the solid-liquid interface measurement method using frequency modulation atomic force microscopy (FM-AFM), that has an atomic resolution in liquid, has made great progress in recent years. Unlike the commonly used method of amplitude modulation AFM, which detects the amplitude change of a cantilever, FM-AFM detects the resonance frequency shift of the cantilever,

thereby achieving high spatial resolution and high sensitivity in detecting force gradients. Initially, FM-AFM imaging in liquid was mainly focused on the solid/water interface, such as the hydration structure on the surface of mica[14–16] and highly oriented pyrolytic graphite.[17] However, recently, molecular scale structures at the interface between liquids other than aqueous solutions, such as ionic liquids, and solids have also been investigated.[18–21] Regarding the structure of the interface between the electrode and solvent used in LIBs, Minato et al. reported that tetraglyme forms a layered structure near the surface of highly oriented pyrolytic graphite.[22] However, there have been no reports on the structure of an electrolyte system containing lithium salt. Here, we investigate the molecular-scale solvation structure formed by the electrolyte near the solid surface of LIBs using FM-AFM and show that the size of the structure formed at the solid-liquid interface increases with increasing ion concentration in the electrolyte. We confirmed that the obtained measurement results are consistent with the Raman spectra and molecular dynamics (MD) simulations. This study strongly suggests that the observed increase in the size of the interfacial structure is due to a change in the effective size of the molecular assembly, that is, the solvated ions.

In this study, we measured the solvation structure of an electrolyte, a solution of lithium bis(trifluoromethanesulfonyl)imide (LiTFSI) in propylene carbonate (PC), at the electrolyte-mica interface. Figure 1 shows the molecular structures and electrostatic potential distributions of PC and TFSI anions. PC is a dipolar aprotic solvent used for nonaqueous electrolytes in LIBs.[23] PC has a negatively charged carbonyl oxygen atom (O_c), as shown in Figs. 1(a) and 1(c), and strongly coordinates with Li ions in the electrolyte. The TFSI anion is a relatively large anion that weakly coordinates to Li ions and forms an air-stable lithium salt (LiTFSI).[24] Although the charge is delocalized within TFSI anions, the nitrogen and oxygen atoms are negatively charged, as shown in Fig. 1(d), and these atoms tend to interact with Li ions. We investigated four LiTFSI salt concentrations in PC: 0, 0.8, 2.1 and 3.6 M. We chose muscovite mica as a model substrate for its atomic smoothness, allowing for high-resolution FM-AFM imaging of its solvation structures.[14–16] While mica is an insulator for Li-ions and different from the surface of real electrodes used in LIBs, it is still an ideal substrate for studying solvation structures formed on the solid/electrolyte interface and has been commonly used in

previous studies.[9,25] In this study, we employed mica substrates to confirm the applicability of FM-AFM for investigating the interfacial structures formed in electrolytes used in LIBs and their concentration dependence.

Raman spectroscopy of bulk LiTFSI-PC electrolytes

Prior to investigating the interfacial solvation structure, Raman spectra of LiTFSI-PC electrolytes were obtained to estimate the interaction between Li^+, PC, and TFSI anions in the bulk electrolyte. As shown in Fig. 2(a), a peak around 710 cm^{-1} was observed in pure PC, which corresponded to the ring deformation of PC.[24] As shown in the inset of Fig. 2(a), the peak at around 710 cm^{-1} showed a shift of the peak position to a higher Raman shift with increasing LiTFSI concentration. The shift of the peak corresponds to a decrease in free PC and an increase in associated PC as a result of the increase in the interaction between PC and Li^+ with increasing LiTFSI concentration.[26] As shown in Fig. 2(b), which shows Raman spectra in the larger wave number region, a peak is observed at around 1225 cm^{-1} for pure PC, which corresponds to the asymmetric stretching of the carbonyl group of PC.[24] With increasing LiTFSI concentration, another peak appeared at approximately 1240 cm^{-1}, which was considered to be caused by the interaction of PC and Li^+. According to structural analysis using density functional theory in a previous study, the oxygen atom protruding from the ring of PC is strongly coordinated to Li^+.[27,28]

We also note that another peak around 740 cm^{-1} appeared with the addition of LiTFSI, as presented in Fig. 2(a). Free anions and solvent-separated ion pairs are commonly characterized by components at 739–742 cm^{-1}, which is attributed to the symmetric deformation of the CF_3 group in the TFSI anion.[24,29] The peak position shifted to the higher Raman shift side with increasing LiTFSI concentration, which is similar to the peak around 710 cm^{-1}, as shown in the inset of Fig. 2(a). This peak shift is attributed to the appearance of the components at higher wavenumbers (> 746 cm^{-1}), which are attributed to contact ion pairs and aggregates.[29] Thus, this suggests a change in the structure of the TFSI anion in solution from solvent-separated ion pairs to contact ion pairs,[26] which means that the TFSI anion interacts with Li ions, although its interaction with Li ions is weaker than that of PC because of charge delocalization of the TFSI anion. These results strongly suggest that Li ions are solvated not only by PC but by TFSI anions, especially in the concentrated LiTFSI-PC electrolyte.

Molecular resolution imaging of interfacial solvation structures

To investigate the solvation structure formed at the interface between the electrolyte and solid, two-dimensional frequency maps were obtained by FM-AFM at the interface between three different concentrations of LiTFSI-PC and mica. First, in the case of pure PC, more than three bright stripes were observed on mica, as shown in the frequency shift maps in Fig. 3(a), which corresponded to the solvation structures that were uniformly formed on the mica surface. The spacing between the stripes was roughly about 0.5 nm, which is close to the average diameter of PC molecules,[30] suggesting that the density distribution of PC is ordered in the direction perpendicular to the mica surface. We converted the frequency shift maps to force maps using the method of Sader and Jarvis.[31] We measured the spacing of the oscillatory force in the force versus distance curves averaged in the direction parallel to the sample surface. The spacings of the force minima were 0.48, 0.51, and 0.54 nm, which were gradually increasing as a function of the distance from the mica surface. We also note that the magnitude of the oscillatory solvation force gradually decreases as a function of distance. These observations suggest that the PC molecules closest to the mica are strongly bound to the mica surface, forming the first uniform layer, as well as the water molecules on the mica surface.[14–16] The increase in the spacing and decrease in the magnitude of the oscillatory force suggest that the interaction between PC molecules and the mica substrate and the layering of PC molecules gradually decrease with increasing distance from the mica surface, and the orientation of PC molecules approaches random.

The force versus distance curves measured at the PC/mica interface at 0.8 and 3.6 M LiTFSI concentrations are shown in Figs. 3(e) and 3(f). Note that the origin of the distance axis in Figs. 3(d)-3(f) is arbitrary. In the average force curve for 0.8 M LiTFSI in Fig. 3(e), there is only one force minimum near the mica surface. However, we found an inflection point at approximately 0.84 nm outside the position of the force minimum. In the case of 3.6 M LiTFSI, as shown in Fig. 3(f), the distance between the two force minima was approximately 1.44 nm. In both cases, the spacing is larger than the size of PC molecules, suggesting that the stripes in Fig. 3(b) and Fig. 3(c) correspond to the layers of the molecular assembly whose size is greater than that of PC molecules. In solvation structure measurements by AFM, the repulsive force is generally attributed to the steric expulsion of

the molecules by the tip. Therefore, we consider that the distance between the onset of the repulsive force corresponds to the thickness of the layer of the molecular assembly. We also note that the dependence of the interlayer distance observed in the force-distance curves as a function of the molarity is mainly due to changes in the mass profile and not due to the charge density profile. Since the cantilever tip we used (SiO_2) was slightly negatively charged but almost neutral and the charge density variation in the solution was small due to the solvation of Li^+ and anions, we consider that the influence of charge density distribution is not significant enough in our experiments. While the competition between mass and charge density profiles on AFM data was discussed in a previous study,[32] we believe that the influence of charge density distribution does not need to be considered in our experiment.

Solvation structures of bulk LiTFSI-PC electrolytes

We first performed MD simulations of the bulk LiTFSI-PC liquid to understand the solvation structure of LiTFSI salt by PC molecules in a 0.8 M LiTFSI-PC solution, the results of which are shown in Fig. 4. As shown in the radial distribution function around Li ions in Fig. 4(a), the oxygen atom of the carbonyl group (O_c) of PC is coordinated to the nearest neighbor of Li ions. As for the TFSI anion, both the oxygen and nitrogen atoms in the anion structure coordinate with Li^+. The coordination number of the O_c of PC and the nitrogen atoms of TFSI anion at a distance of 0.3 nm from Li ions are approximately 3.6 and 0.8, respectively. Since there is only one nitrogen atom in the $TFSI^-$ and the coordination number of the nitrogen atom corresponds to the coordination number of the $TFSI^-$ around Li^+, it is indicated that Li ions are dominantly solvated by PC in the LiTFSI-PC electrolyte at a concentration of 0.8 M while there is some contribution from the solvation structure containing a TFSI anion in its first solvation shell. Based on the coordination number, several coordinating structures with three or four PCs coordinated to Li^+ coexist in the electrolyte. We presume that the molecular assemblies that may be formed in an electrolyte of 0.8 M LiTFSI in PC include Li^+-$(PC)_3$, Li^+-$(PC)_4$, Li^+-$(PC)_3$-$TFSI^-$ and Li^+-$(PC)_4$-$TFSI^-$. Figures 4(b–d) show representative molecular assemblies of Li ions coordinated by PC molecules and a TFSI anion, taken from snapshots of the MD simulation. As mentioned above, Raman spectroscopy measurements suggest that a molecular assembly, in which both PC and TFSI anions are

coordinated to Li ions, is formed in the LiTFSI-PC electrolyte, and the results obtained by the MD simulation are also consistent with this.

Interfacial structures at mica/ LiTFSI-PC electrolytes

We then performed an MD simulation of the interface between the electrolyte of 0.8 M LiTFSI in PC and mica, as shown in Fig. 5(a). Figure 5(b) shows the density distribution profiles of the ions and PC molecules as a function of the distance from the electrolyte/mica interface, which were calculated from snapshots of the MD simulations. It shows that there is an oscillation with a spacing of approximately 0.5 nm in the density distribution profile of the electrolyte, which mainly reflects the density distribution profile of PC molecules. In fact, it is very similar to the density distribution profile of pure PC (see Fig. S2). This is because even in the 0.8 M LiTFSI electrolyte, the number of PC molecules is still approximately 14 times larger than the number of LiTFSI molecules. In particular, the peak at approximately 0.3 nm from the mica is almost entirely due to PC, and the ratio of Li ions to TFSI anions at this position is very small. There is also a shoulder peak at approximately 0.4 nm, as indicated by the gray arrow in Fig. 5(b). This is because the PC molecules in this region were oriented in two ways. Namely, there were PC molecules with the oxygen atoms of the carbonyl groups facing the mica surface, giving a peak at 0.3 nm, and those with the hydrogen atoms facing the mica substrate, giving a shoulder peak at 0.4 nm (see Fig. S3). In a previous study by sum-frequency generation, it was shown that PC molecules are oriented in two ways at the PC/$LiCoO_2$ interface,[33] which is similar to our result. Moreover, focusing on the density distribution of Li ions, a sharp peak was observed at 0.8 nm from the mica surface. The density of Li ions at this position was more than three times higher than the mean density of Li ions in the bulk region, which was greater than 3 nm from the mica surface. Furthermore, the distribution of TFSI anions was less pronounced than that of Li ions, although a small peak was observed around 0.8 nm from the mica. These distributions suggest that there is a local excess of positive charges in the electrolyte in the region near the negatively charged mica surface. In addition, these profiles suggest that the positively charged Li ions are not directly adsorbed on the negatively charged mica surface, but have a higher probability of being present at a slightly distant location. We assume that this is because the solvation of Li ions by PC molecules and TFSI anions is

stronger than the electrostatic interaction between bare Li ions and the negatively charged mica surface. In fact, according to snapshots obtained from MD simulations, as shown in Fig. 5(c–e), molecular assemblies including Li^+-$(PC)_3$, Li^+-$(PC)_4$ and Li^+-$(PC)_3$-$TFSI^-$ are formed near the interface. We consider that among these, Li^+-$(PC)_3$ and Li^+-$(PC)_4$ are the major species at the interface, and some contributions from Li^+-$(PC)_3$-$TFSI^-$ are also present. This is because the electrolyte is locally positively charged in this region, as described above, and the positively charged Li^+-$(PC)_3$ and Li^+-$(PC)_4$ are likely in excess of Li^+-$(PC)_3$-$TFSI^-$, which is a charge-neutral molecular assembly. The sizes of Li^+-$(PC)_3$ and Li^+-$(PC)_4$ are in the range of 0.8–1 nm, which is close to the size of the characteristic force oscillation intervals observed in the force curves of FM-AFM. In other words, in the LiTFSI-PC electrolyte, Li ions are strongly solvated by PC and TFSI anions, forming large molecular assemblies, and these molecular assemblies further solvate the mica surface. When the tip disturbs the layers of the molecular assemblies, layering of the molecular assemblies is detected as an oscillatory hydration force with a spacing that corresponds to the size of the molecular assembly. Therefore, by detecting changes in the interaction force, we can estimate the size of the structure formed at the interface. In fact, as shown in Fig. 3, a structure with a characteristic size of 1.44 nm, which is larger than that in the 0.8 M solution, was detected in the 3.6 M solution. It has been considered that larger structures are formed in an electrolyte with a higher concentration of the electrolyte generally used for LIBs.[26,34] This is because ions and other dissolved solute molecules tend to self-assemble into relatively large and polydisperse aggregates.[35] The results presented here are consistent with this tendency. It should be noted that the MD simulations of the electrolyte with the 3.6 M solution did not converge. We believe this is because the force field is not optimized for the combination of mica and electrolyte. For mica and electrolyte on their own, the force field has been optimized as shown in the previous studies.[36–38] We consider that the force fields individually optimized for mica and electrolyte could be used without modification for weak electrolytes, but they should be modified for concentrated electrolytes. Although we could not discuss the structures formed at the mica interface in the case of 3.6 M LiTFSI-PC electrolyte in detail, we could calculate the structure of the molecular assemblies formed at the interface in the electrolyte with a high concentration using other calculation methods in the future, such as the reference interaction site model

or first-principles MD simulations. Note that the desolvation energies of the two structures, Li^+-$(PC)_3$ and Li^+-$(PC)_4$, which are thought to be dominant at the interface between the LiTFSI electrolyte and mica at a concentration of 0.8 M, are related to the origin of the interfacial resistance of LIBs. In the desolvation process of these structures, PC molecules are removed from the solvated clusters, and the desolvation energy when the last PC molecule is removed from the Li ion can be obtained by DFT calculation.[6] Although the measurement was performed using mica in this study, it would be possible to discuss the origin of the interfacial resistance of the LIB by analyzing the interface between the electrode material and the electrolyte used in a LIB using FM-AFM and MD simulations, and by determining the desolvation energy of the estimated solvation structure at the interface using DFT.

Finally, we note that the major advantage of FM-AFM is that it can be used to investigate interfacial structures even with highly concentrated electrolytes. Because the viscosity of the liquid increased significantly with high electrolyte concentration, the Q value of the cantilever vibration spectrum decreased significantly in the FM-AFM measurement, and the vibration spectrum became very broad (Figure S4). In FM-AFM, which measures the shift in the resonant frequency of the cantilever vibration, the measurement becomes more difficult because the force detection sensitivity decreases as the Q value of the vibration spectrum decreases. However, in this study, structural changes at the solid-liquid interface could be detected on a molecular scale, even when a high-concentration (3.6 M) LiTFSI-PC solution was used. This clearly indicates that FM-AFM has a high potential for structural measurements at the electrolyte-solid interface of LIBs. Additionally, in this study, we mainly discussed the one-dimensional distribution of electrolytes in the direction perpendicular to the mica surface, but FM-AFM has the potential to measure the distribution of liquids in two and three dimensions. Therefore, it is possible, in principle, to discuss the adsorption and orientation of molecules to individual atoms on a solid surface, which is our future work. We also note that the FM-AFM measurements shown in this study can also be performed using solvents such as a mixture of EC and DMC, which are the most common electrolyte solutions for LIBs.

The molecular-scale solvation structures formed near the interface between the LiTFSI-PC electrolyte used

in LIBs and mica were measured using FM-AFM. The characteristic force oscillation spacings in the force curves increased with increasing LiTFSI concentration in the electrolyte, suggesting an increase in the effective size of molecules at the solid-liquid interface. MD simulations showed that molecular assemblies including Li^+-$(PC)_3$, Li^+-$(PC)_4$, and Li^+-$(PC)_3$-$TFSI^-$ were formed at the interface. The sizes of these structures are close to the spacing of the characteristic force oscillations in the force curves. The combined method of molecular-scale solid-liquid interface measurement using FM-AFM and MD simulation is expected to play an important role in elucidating the structure of molecular assemblies formed by ions and molecules at the solid-liquid interfaces in electrolytes used in energy devices in the future.

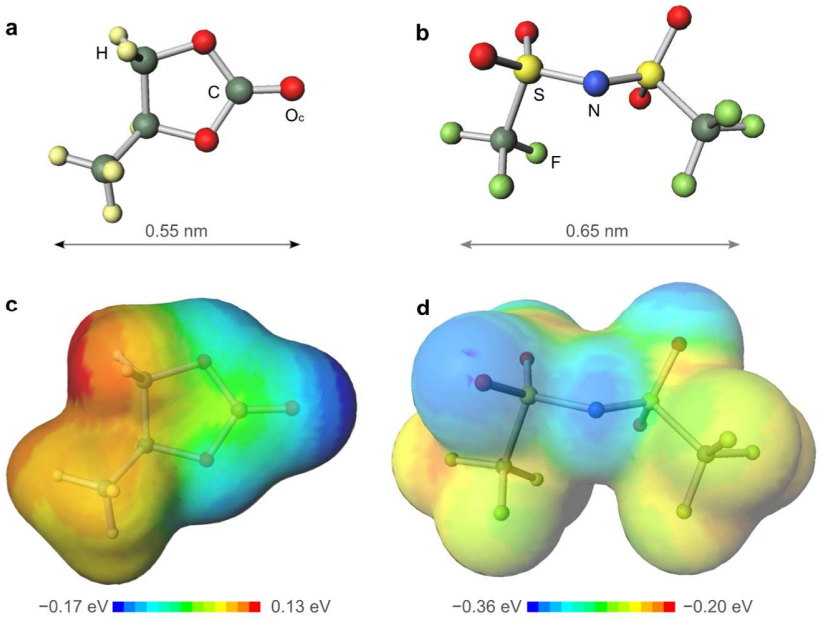

Figure 1. Molecular structures of (a) PC and (b) TFSI anion with the lowest energy conformation, optimized using the B3LYP/6-31G* function. The arrows indicate the average diameter of PC[30] and the ionic radius of TFSI anion dissolved in PC.[23] (c–d) Three-dimensional distributions of electrostatic potential drawn on their electron density isosurfaces at 10.7 e/nm^3.

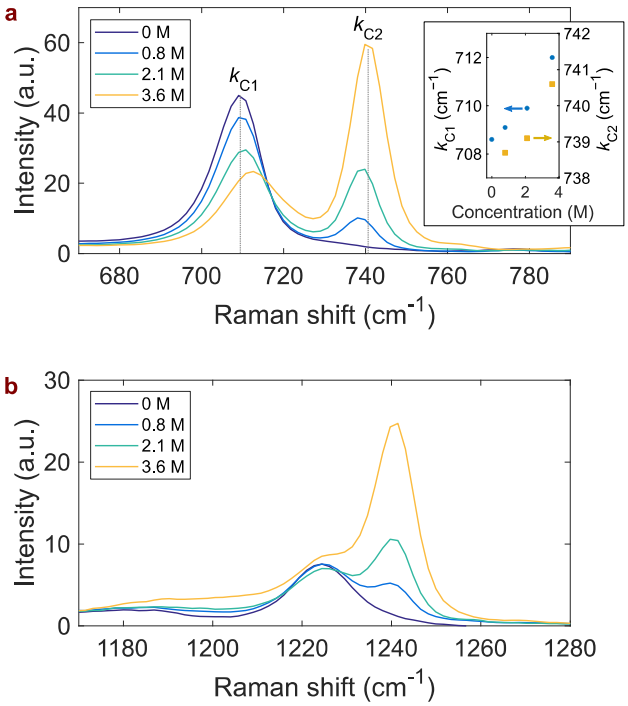

Figure 2. (a–b) Raman spectra of LiTFSI-PC electrolytes with different concentrations measured in two different wave number regions. Inset in (a) shows the concentration dependence of the center values of the two peaks in the spectrum.

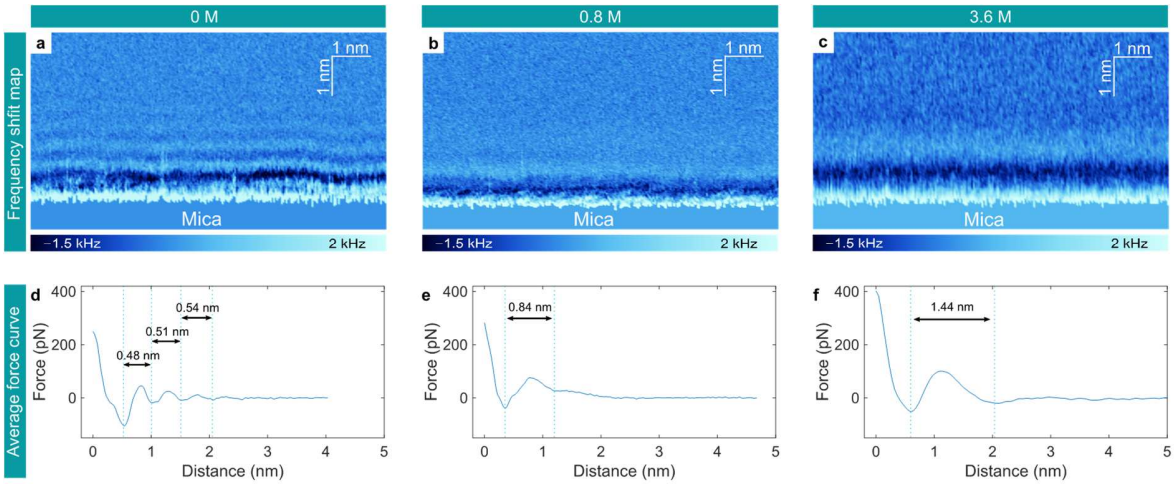

Figure 3. (a–c) Two-dimensional frequency shift maps obtained at the interface between mica and LiTFSI-PC solutions of different concentrations (0, 0.8, and 3.6 M). (d–f) Averaged force curves obtained by averaging the force curves in the force maps converted from the frequency shift maps shown in the upper panel.

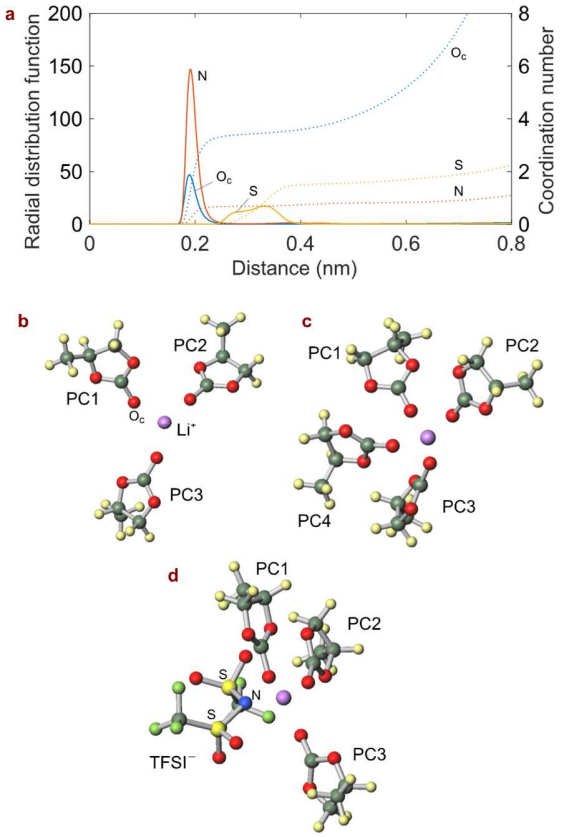

Figure 4. (a) Radial distribution functions (solid curves) and coordination numbers (dashed curves) for 0.8 M LiTFSI-PC electrolytes calculated by MD simulations. Representative snapshots from MD simulations illustrating molecular assemblies in the bulk 0.8 M LiTFSI-PC electrolyte. (b) Li^+-$(PC)_3$. (c) Li^+-$(PC)_4$. (d) Li^+-$(PC)_3$-$TFSI^-$.

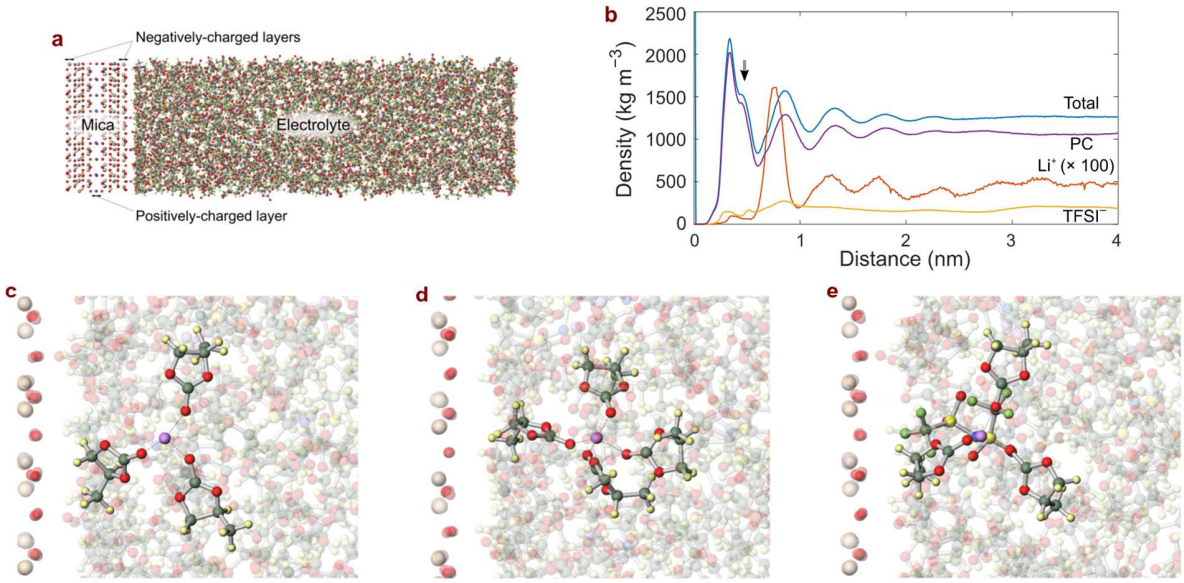

Figure 5. (a) Representative cell structure used for molecular dynamics simulations of the mica/electrolyte interfaces. (b) Density distribution of electrolyte at 0.8 M LiTFSI-PC electrolyte/mica interface. Representative snapshots from MD simulations illustrating the interfacial solvation structures of Li ion with different compositions at the 0.8M LiTFSI-PC electrolyte/mica interface. (c) Li^+-$(PC)_3$. (d) Li^+-$(PC)_4$. (e) Li^+-$(PC)_3$-$TFSI^-$.

ASSOCIATED CONTENT

Supporting Information. The Supporting Information is available free of charge at the URL.

Materials and methods, additional Raman spectra of LiTFSI-PC electrolytes, additional data from MD simulations, and representative frequency spectra of cantilever Brownian motion in LiTFSI-PC solutions.

AUTHOR INFORMATION

Corresponding Author

Yuji Yamagishi-Applied Materials Technology Center, Technology Division, Panasonic Holdings Corporation, 3-1-1 Yagumo-nakamachi, Moriguchi, Osaka 570-8501, Japan

E-mail: yamagishi.yuji001@jp.panasonic.com

Notes

The authors declare no competing financial interests.

ACKNOWLEDGMENT

The authors would like to thank Dr. Masaki Okoshi at Panasonic for advice on the MD simulation of electrolytes in LIBs. This research did not receive any specific grants from funding agencies in the public, commercial, or not-for-profit sectors.

REFERENCES

(1) Atkins, D.; Ayerbe, E.; Benayad, A.; Capone, F. G.; Capria, E.; Castelli, I. E.; Cekic-Laskovic, I.; Ciria, R.; Dudy, L.; Edström, K.; Johnson, M. R.; Li, H.; Lastra, J. M. G.; De Souza, M. L.; Meunier, V.; Morcrette, M.; Reichert, H.; Simon, P.; Rueff, J.; Sottmann, J.; Wenzel, W.; Grimaud, A. Understanding Battery Interfaces by Combined Characterization and Simulation Approaches: Challenges and Perspectives. *Adv. Energy Mater.* **2021**, *2102687*, 2102687. https://doi.org/10.1002/aenm.202102687.

(2) Minato, T.; Abe, T. Surface and Interface Sciences of Li-Ion Batteries: -Research Progress in Electrode–

Electrolyte Interface-. *Prog. Surf. Sci.* **2017**, *92* (4), 240–280. https://doi.org/10.1016/j.progsurf.2017.10.001.

(3) Cheng, H.; Sun, Q.; Li, L.; Zou, Y.; Wang, Y.; Cai, T.; Zhao, F.; Liu, G.; Ma, Z.; Wahyudi, W.; Li, Q.; Ming, J. Emerging Era of Electrolyte Solvation Structure and Interfacial Model in Batteries. *ACS Energy Lett.* **2022**, 490–513. https://doi.org/10.1021/acsenergylett.1c02425.

(4) Abe, T.; Sagane, F.; Ohtsuka, M.; Iriyama, Y.; Ogumi, Z. Lithium-Ion Transfer at the Interface Between Lithium-Ion Conductive Ceramic Electrolyte and Liquid Electrolyte-A Key to Enhancing the Rate Capability of Lithium-Ion Batteries. *J. Electrochem. Soc.* **2005**, *152* (11), A2151. https://doi.org/10.1149/1.2042907.

(5) Abe, T.; Fukuda, H.; Iriyama, Y.; Ogumi, Z. Solvated Li-Ion Transfer at Interface Between Graphite and Electrolyte. *J. Electrochem. Soc.* **2004**, *151* (8), A1120. https://doi.org/10.1149/1.1763141.

(6) Okoshi, M.; Soc, J. E.; Okoshi, M.; Yamada, Y.; Yamada, A.; Nakai, H. Theoretical Analysis on De-Solvation of Lithium, Sodium, and Magnesium Cations to Organic Electrolyte Solvents. *J. Electrochem. Soc.* **2013**, *160* (11). https://doi.org/10.1149/2.074311jes.

(7) Regan, M. J.; Kawamoto, E. H.; Lee, S.; Pershan, P. S.; Maskil, N.; Deutsch, M.; Magnussen, O. M.; Ocko, B. M.; Berman, L. E. Surface Layering in Liquid Gallium: An X-Ray Reflectivity Study. *Phys. Rev. Lett.* **1995**, *75* (13), 2498–2501. https://doi.org/10.1103/PhysRevLett.75.2498.

(8) Cheng, L.; Fenter, P.; Nagy, K. L.; Schlegel, M. L.; Sturchio, N. C. Molecular-Scale Density Oscillations in Water Adjacent to a Mica Surface. *Phys. Rev. Lett.* **2001**, *87* (15), 156103. https://doi.org/10.1103/PhysRevLett.87.156103.

(9) Steinrück, H. G.; Cao, C.; Tsao, Y.; Takacs, C. J.; Konovalov, O.; Vatamanu, J.; Borodin, O.; Toney, M. F. The Nanoscale Structure of the Electrolyte-Metal Oxide Interface. *Energy Environ. Sci.* **2018**, *11* (3), 594–602. https://doi.org/10.1039/c7ee02724a.

(10) Liu, H.; Tong, Y.; Kuwata, N.; Osawa, M.; Kawamura, J. Adsorption of Propylene Carbonate (PC) on the $LiCoO_2$ Surface Investigated by Nonlinear Vibrational Spectroscopy. *J. Phys. Chem. C* **2009**, *113*, 20531–20534.

(11) Nicolau, B. G.; Garc, N.; Dryzhakov, B.; Dlott, D. D. Interfacial Processes of a Model Lithium Ion Battery Anode Observed, in Situ, with Vibrational Sum-Frequency Generation Spectroscopy. *J. Phys. Chem. C* **2015**, *119*, 10227–10233. https://doi.org/10.1021/acs.jpcc.5b01290.

(12) Chowdhury, A. U.; Muralidharan, N.; Daniel, C.; Amin, R.; Belharouak, I. Probing the Electrolyte/Electrode Interface with Vibrational Sum Frequency Generation Spectroscopy: A Review☆. *J. Power Sources* **2021**, *506*, 230173. https://doi.org/10.1016/j.jpowsour.2021.230173.

(13) Gao, Q.; Tsai, W.; Balke, N. In Situ and Operando Force-based Atomic Force Microscopy for Probing Local Functionality in Energy Storage Materials. *Electrochem. Sci. Adv.* 2022, *2* (1), e2100038. https://doi.org/10.1002/elsa.202100038.

(14) Fukuma, T.; Ueda, Y.; Yoshioka, S.; Asakawa, H. Atomic-Scale Distribution of Water Molecules at the Mica-Water Interface Visualized by Three-Dimensional Scanning Force Microscopy. *Phys. Rev. Lett.* **2010**, *104* (1), 2–5. https://doi.org/10.1103/PhysRevLett.104.016101.

(15) Kimura, K.; Ido, S.; Oyabu, N.; Kobayashi, K.; Hirata, Y.; Imai, T.; Yamada, H. Visualizing Water Molecule Distribution by Atomic Force Microscopy. *J. Chem. Phys.* **2010**, *132* (19). https://doi.org/10.1063/1.3408289.

(16) Kobayashi, K.; Oyabu, N.; Kimura, K.; Ido, S.; Suzuki, K.; Imai, T.; Tagami, K.; Tsukada, M.; Yamada, H. Visualization of Hydration Layers on Muscovite Mica in Aqueous Solution by Frequency-Modulation Atomic Force Microscopy. *J. Chem. Phys.* **2013**, *138* (18). https://doi.org/10.1063/1.4803742.

(17) Suzuki, K.; Oyabu, N.; Kobayashi, K.; Matsushige, K.; Yamada, H. Atomic-Resolution Imaging of Graphite-Water Interface by Frequency Modulation Atomic Force Microscopy. *Appl. Phys. Express* **2011**, *4* (12), 2–5. https://doi.org/10.1143/APEX.4.125102.

(18) Black, J. M.; Zhu, M.; Zhang, P.; Unocic, R. R.; Guo, D.; Okatan, M. B.; Dai, S.; Cummings, P. T.; Kalinin, S. V.; Feng, G.; Balke, N. Fundamental Aspects of Electric Double Layer Force-Distance Measurements at Liquid-Solid Interfaces Using Atomic Force Microscopy. *Sci. Rep.* **2016**, *6* (1), 1–12.

https://doi.org/10.1038/srep32389.

(19) Umeda, K.; Kobayashi, K.; Minato, T.; Yamada, H. Molecular-Scale Solvation Structures of Ionic Liquids on a Heterogeneously Charged Surface. *J. Phys. Chem. Lett.* **2020**, *11* (19), 8094–8099. https://doi.org/10.1021/acs.jpclett.0c02356.

(20) Zhou, S.; Panse, K. S.; Motevaselian, M. H.; Aluru, N. R.; Zhang, Y. Three-Dimensional Molecular Mapping of Ionic Liquids at Electrified Interfaces. *ACS Nano* **2020**, *14*, 17515–17523. https://doi.org/10.1021/acsnano.0c07957.

(21) Bao, Y.; Kitta, M.; Ichii, T.; Utsunomiya, T.; Sugimura, H. Visualization of Solvation Structure on $Li_4Ti_5O_{12}$(111)/ Ionic Liquid-Based Electrolyte Interface by Atomic Force Microscopy. *Jpn. J. Appl. Phys.* **2021**, *60*, SE1004.

(22) Minato, T.; Araki, Y.; Umeda, K.; Yamanaka, T.; Okazaki, K. I.; Onishi, H.; Abe, T.; Ogumi, Z. Interface Structure between Tetraglyme and Graphite. *J. Chem. Phys.* **2017**, *147* (12). https://doi.org/10.1063/1.4996226.

(23) Ue, M. Mobility and Ionic Association of Lithium and Quaternary Ammonium Salts in Propylene Carbonate and γ- Butyrolactone. *J. Electrochem. Soc.* **1994**, *141*, 3336.

(24) Wang, Z.; Gao, W.; Huang, X.; Mo, Y.; Chen, L. Spectroscopic Studies on Interactions and Microstructures in Propylene Carbonate — LiTFSI Electrolytes. *J. Raman Spectrosc.* **2001**, *32*, 900–905.

(25) Han, M.; Zhang, R.; Gewirth, A. A.; Espinosa-Marzal, R. M. Nanoheterogeneity of LiTFSI Solutions Transitions Close to a Surface and with Concentration. *Nano Lett.* 2021, *21* (5), 2304–2309. https://doi.org/10.1021/acs.nanolett.1c00167.

(26) Chang, Z.; Qiao, Y.; Yang, H.; Deng, H.; Zhu, X.; He, P.; Zhou, H. Beyond the Concentrated Electrolyte: Further Depleting Solvent Molecules within a Li^+ Solvation Sheath to Stabilize High-Energy-Density Lithium Metal Batteries. *Energy Environ. Sci.* **2020**, *13* (11), 4122–4131. https://doi.org/10.1039/D0EE02769C.

(27) Chapman, N.; Borodin, O.; Yoon, T.; Nguyen, C. C.; Lucht, B. L. Spectroscopic and Density Functional Theory

Characterization of Common Lithium Salt Solvates in Carbonate Electrolytes for Lithium Batteries. *J. Phys. Chem. C* **2017**, *121* (4), 2135–2148. https://doi.org/10.1021/acs.jpcc.6b12234.

(28) Bhatt, M. D.; Cho, M.; Cho, K. Conduction of Li^+ Cations in Ethylene Carbonate (EC) and Propylene Carbonate (PC): Comparative Studies Using Density Functional Theory. *J. Solid State Electrochem.* **2012**, *16* (2), 435–441. https://doi.org/10.1007/s10008-011-1350-7.

(29) Herstedt, M.; Smirnov, M.; Johansson, P.; Chami, M.; Grondin, J.; Servant, L.; Lassègues, J. C. Spectroscopic Characterization of the Conformational States of the Bis(Trifluoromethanesulfonyl)Imide Anion ($TFSI^-$). *J. Raman Spectrosc.* **2005**, *36* (8), 762–770. https://doi.org/10.1002/jrs.1347.

(30) Marcus, Y. *The Properties of Solvents*; Wiley, 1999.

(31) Sader, J. E.; Jarvis, S. P. Accurate Formulas for Interaction Force and Energy in Frequency Modulation Force Spectroscopy. *Appl. Phys. Lett.* **2004**, *84*, 1801. https://doi.org/10.1063/1.1667267.

(32) Benaglia, S.; Uhlig, M. R.; Hernández-Muñoz, J.; Chacón, E.; Tarazona, P.; Garcia, R. Tip Charge Dependence of Three-Dimensional AFM Mapping of Concentrated Ionic Solutions. *Phys. Rev. Lett.* 2021, *127* (19), 196101. https://doi.org/10.1103/PhysRevLett.127.196101.

(33) Peng, Q.; Liu, H.; Ye, S. Adsorption of Organic Carbonate Solvents on a Carbon Surface Probed by Sum Frequency Generation (SFG) Vibrational Spectroscopy. *J. Electroanal. Chem.* **2017**, *800*, 134–143. https://doi.org/10.1016/j.jelechem.2016.09.006.

(34) Yamada, Y.; Wang, J.; Ko, S.; Watanabe, E.; Yamada, A. Advances and Issues in Developing Salt-Concentrated Battery Electrolytes. *Nat. Energy* **2019**, *4*, 269–280. https://doi.org/10.1038/s41560-019-0336-z.

(35) McOwen, D. W.; Seo, D. M.; Borodin, O.; Vatamanu, J.; Boyle, P. D.; Henderson, W. A. Concentrated Electrolytes: Decrypting Electrolyte Properties and Reassessing Al Corrosion Mechanisms. *Energy Environ. Sci.* **2014**, *7* (1), 416–426. https://doi.org/10.1039/c3ee42351d.

(36) Soetens, J. C.; Millot, C.; Maigret, B. Molecular Dynamics Simulation of $Li^+BF_4^-$ in Ethylene Carbonate, Propylene Carbonate, and Dimethyl Carbonate Solvents. *J. Phys. Chem. A* **1998**, *102* (7), 1055–1061. https://doi.org/10.1021/jp972457+.

(37) Lopes, J. N. C.; Pádua, A. A. H. Molecular Force Field for Ionic Liquids Composed of Triflate or Bistriflylimide Anions. *J. Phys. Chem. B* **2004**, *108* (43), 16893–16898. https://doi.org/10.1021/jp0476545.

(38) Cygan, R. T.; Liang, J.; Kalinichev, A. G. Molecular Models of Hydroxide , Oxyhydroxide , and Clay Phases and the Development of a General Force Field. *J. Phys. Chem. B* **2004**, *108*, 1255–1266.